Pure Appl. Chem., Vol. 85, No. 2, pp. 453–462, 2013.
http://dx.doi.org/10.1351/PAC-CON-12-08-12

Impact of sintering temperature on the phase composition and antibacterial properties of silver-doped hydroxyapatite*

Arita Dubnika[1,‡], Dagnija Loca[1], Aigars Reinis[2], Maris Kodols[3], and Liga Berzina-Cimdina[1]

[1]Rudolfs Cimdins Riga Biomaterials Innovation and Development Centre, Riga Technical University, Pulka 3/3, LV-1007, Riga, Latvia; [2]Department of Biology and Microbiology, Riga Stradins University, Dzirciema 6, LV-1007, Riga, Latvia; [3]Institute of Inorganic Chemistry, Riga Technical University, Miera Str. 34, Salaspils, LV-2169, Latvia

Abstract: In the present study, the impact of sintering temperature on the phase composition and antibacterial properties of silver-doped hydroxyapatite (HAp/Ag) samples was investigated. HAp/Ag containing 0.2 and 1.2 % silver was prepared using a modified wet chemical precipitation method. The surface morphology and inner structure of the sintered samples were discussed. X-ray powder diffraction (XRD) and scanning electron microscopy (SEM) studies showed that, after the sintering process, HAp/Ag contained a silver oxide phase, which was not observed in raw materials. Phase composition changes at different sintering temperatures were studied, and it was found that silver oxide undergoes phase changes during the sintering process. In vitro antibacterial properties approved the excellent antimicrobial activity of HAp/Ag against the bacterial strains *Staphylococcus epidermidis* and *Pseudomonas aeruginosa*. The HAp/Ag sample with 1.2 % silver content, sintered at 1150 °C, showed the highest antibacterial activity.

Keywords: antimicrobial activity; biomaterials; ceramics; hydroxyapatite; silver; phase transitions.

INTRODUCTION

Biomaterials based on calcium orthophosphates are widely used for medical applications due to their osteoconductivity, bioactivity, and biocompatibility. The main mineral component of bone and hard tissues is hydroxyapatite (HAp), which contains several ionic substituents in the crystalline lattice, such as CO_3^{2-}, F^-, Mg^{2+}, Na^+, etc. The chemical composition and structure of synthetic HAp are similar to bone and teeth mineral components, which is why HAp is used in different biomedical applications for hard tissue regeneration as an implant material [1–3]. Implantation is often associated with bacterial infections, which can lead to complications; therefore, materials with good osteoconductive and antibacterial properties are desired [4]. Metal ions like Ag^+, Cu^{2+}, and Zn^{2+} are used for incorporation in the HAp structure as antibacterial agents. Cationic substitutions are possible due to the high stability and flexibility of the HAp structure [5]. Silver and silver ions have been used in medicine for anti-

Pure Appl. Chem. **85**, 315–462 (2013). A collection of invited papers based on presentations at the 12th Eurasia Conference on Chemical Sciences, Corfu, Greece, 16–21 April 2012.
‡Corresponding author

bacterial purposes for a long time [6,7]. Silver has a broad spectrum of antibacterial properties, which are essential for the bacterial infections related to implantation [8]. The combination of silver antibacterial properties and HAp biocompatibility opens up new opportunities for promising biomaterials in the field of hard tissue regeneration [9–11].

In several studies, the synthesis of HAp/Ag has been described by using different processes. Kim et al. [12] synthesized silver ion substituted HAp by the wet precipitation method, using calcium hydroxide and phosphoric acid as raw materials and determined the phase composition and antibacterial properties for unsintered material. Chung et al. [13] developed a sol-gel procedure for obtaining the mixed crystal; the derived products were sintered at different temperatures from 250 to 650 °C, and the sintered powders were used for pallet preparation and antibacterial tests. For both of these methods, an Ag_2O phase was observed besides the HAp and HAp/Ag phases. Different methods for obtaining silver nanoparticles onto a nano HAp surface can be found in the literature, but the sintering temperature for the powders does not exceed 350 °C [14–16]. To prevent the formation of Ag_2O and to obtain the desired HAp/Ag, where calcium ions are replaced with silver ions, Stanic et al. [17] and Singh et al. [18] have developed two different modified wet precipitation methods. Singh et al. [18] sintered samples at 1200 °C and used them for the determination of phase composition and antibacterial activity, but the changes of phase composition and antibacterial properties, depending on the sintering temperature, were not discussed. The preparation of HAp/Ag has an essential meaning because its crystalline structure influences thermodynamic, mechanical, and antibacterial properties [19].

Many publications on the subject of silver-substituted HAp preparation and characterization can be found, but only few of them [18,19] explain the phase transfer, phase composition, and other events during sintering. Only some information can be found about the antimicrobial properties of HAp/Ag bioceramic samples, with respect to sintering temperature and the location of silver in these samples. Therefore, the aim of this study was to obtain the HAp/Ag mixed crystal, determine the phase composition of sintered powders and scaffolds, explain the phase transition during the sintering, and elucidate the effect of the sintering temperature on the antibacterial activity of the prepared samples. In the current research, HAp/Ag was prepared, using a modified wet chemical method [20,21]. All the samples were sintered as scaffolds and powders at two different temperatures, 1000 and 1150 °C, to determine the phase composition changes by the XRD. *Staphylococcus epidermidis* and *Pseudomonas aeruginosa* bacterial strains were chosen to evaluate the in vitro antibacterial activity of the prepared samples.

MATERIALS AND METHODS

Synthesis of HAp/Ag

Reference HAp and HAp/Ag samples were synthesized using a modified wet chemical method. The precursors used for HAp synthesis included calcium oxide (≥97 %, FLUKA), phosphoric acid (85.5 %, Sigma Aldrich), and silver nitrate (≥99 %, Sigma Aldrich). Deionized water was used for all experiments. All synthesis was made with the amount [Ca + Ag] = 0.25 mol and the atomic ratio (Ca + Ag)/P fixed at 1.67. Silver nitrate was added in an appropriate amount with atomic ratios Ag/(Ag + Ca) = 0 (HAp); 0.002 (HAp/Ag1) and 0.012 (HAp/Ag2). $Ca(OH)_2$ (0.25 mol/L) suspension was prepared by milling the required amount of CaO in 200 mL of water in a ball mill. The required amount of $AgNO_3$ was dissolved in water (0.01 mol/L). In correct proportions, silver nitrate solution was added to the calcium hydroxide suspension and heated to 90 °C with continuous stirring. Phosphoric acid (2 M) was added dropwise to the suspension. The obtained suspension was aged for 15 h, filtered, and dried at 100 °C. Samples were sintered as powders and scaffolds to determine the phase composition changes after sintering. Before sintering, powders were uniaxially pressed in 2-mm-thick scaffolds (with the diameter 10 mm). The sintering of samples was carried out at 1000 and 1150 °C for 2 h.

Characterization of the materials

HAp powders and scaffolds were analyzed by X-ray powder diffraction (XRD, PANalytical zX'Pert Pro diffractometer, The Netherlands) using Cu Kα radiation at 40 kV and 30 mA, 2θ range of 10–55°. The obtained pattern was compared with the pattern from the literature [22]. The porosity was determined with the Archimedes method. To determinate the silver content of the powder samples, X-ray fluorescence spectrometry (XRF, BRUKER, Pioneer S4) was used. Scanning electron microscopy (SEM) was used to evaluate the surface morphology and inner structure of the prepared composites. Samples were sputter-coated with gold using a fine coat ion sputter device, and observed using a Tescan Mira/LMU scanning electron microscope.

Determination of in vitro antimicrobial properties

In the study, reference cultures of *S. epidermidis* ATCC 12228 and *P. aeruginosa* ATCC 27853 were used. *S. epidermidis* is a Gram-positive facultative anaerobic coccus, but *P. aeruginosa* is a Gram-negative facultative anaerobic rod. Both organisms are capable of biofilm formation on implant surfaces [23–25]. Bacteria suspensions were prepared from the microbiological cultures in 1 mL of TSB (Triptycase soy broth, Oxoid, UK) with the concentrations of 10, 10^2, 10^3 CFU/mL (colony forming units). For determination of bacteria adhesion, samples were cultivated at 37 °C for 2 h. HAp/Ag and HAp samples were incubated in 1 mL of TSB for 24 h, to evaluate the level of the microorganism colonization. For determination of both bacteria adhesion and colonization, the sonication-plate count method [26,27] was used. The unattached microorganisms were washed off after incubation. To separate the bacteria attached on the sample surface, samples were treated in an ultrasonic bath for 1 min (with a frequency of 45 kHz) and for 1 min in a centrifuge Vortex at maximum rotational speed. Several subcultures were prepared on a TSA growth medium (Triptycase soy agar, Oxoid, UK), cultivated for 24 h at a temperature of 37 °C, to determine the total count of microorganisms. For CFU calculations, 1 mm^2 of the biomaterial sample surface was used. Samples for SEM analysis were fixed in a mixture of ether-ethanol (1:1).

Statistics

Results are represented as the mean value ±SD (standard deviation) of three experiments. Statistical analysis was done on adhesion and colonization intensity data with unpaired Student's t-test and $p < 0.05$ was used as a limit to indicate statistical significance.

RESULTS AND DISCUSSION

Characterization and phase composition of HAp/Ag

Changes in the HAp/Ag1 particle morphology after the sintering process are shown in Fig. 1. These images clearly indicate the particle agglomeration during sintering. Dried and milled HAp/Ag particles before sintering were more rounded, and the length of particles was in the range from 20 to 65 nm. The length of the particles sintered at 1000 °C was in the range of 70 to 200 nm, which is approximately three times more than that for unsintered particles. Particles sintered at 1150 °C were agglomerated in larger clusters, and the crystallinity of the material increased.

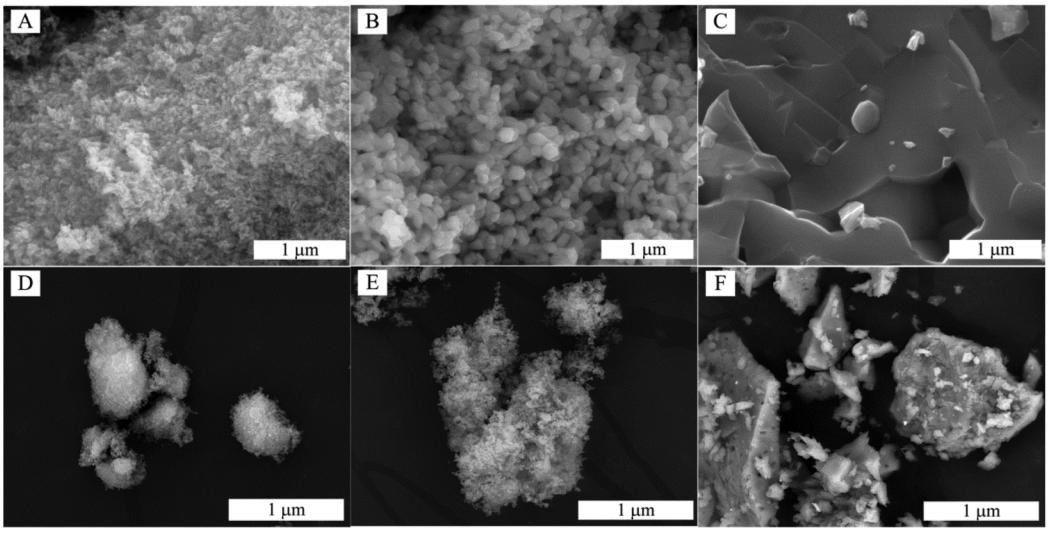

Fig. 1 SEM images of HAp/Ag1 particles: (A, D) unsintered, (B, E) sintered at 1000 °C and (C, F) sintered at 1150 °C.

For determination of the silver amount, XRF analysis was used. XRF results (Table 1) showed that the silver amount was decreasing with an increase in the sintering temperature. Significant differences in the silver amount were observed between powder samples and scaffolds, which can be explained by the differences in the surface areas.

Table 1 Changes in the silver amount during the sintering process.

HAp/Ag1	Ag (%)	HAp/Ag2	Ag (%)
Unsintered material	0.20	Unsintered material	1.20
Powder (1000 °C)	0.19	Powder (1000 °C)	1.18
Powder (1150 °C)	0.17	Powder (1150 °C)	0.89
Scaffold (1000 °C)	0.19	Scaffold (1000 °C)	1.18
Scaffold (1150 °C)	0.18	Scaffold (1150 °C)	1.13

During sintering, at first, silver recrystallizes on the surface of HAp particles, then it evaporates from the surface with increasing sintering temperature (Fig. 2). Silver oxide can be seen on the surface of HAp/Ag powder particles and at the fracture of sintered scaffolds, but silver oxide crystals were not determined on the surface of sintered scaffolds (Fig. 2). The porosity of sintered HAp/Ag scaffolds and pure HAp scaffolds treated in the same conditions was evaluated. The results showed that open porosity of HAp/Ag scaffolds was 32–35 % and that of HAp scaffolds 40–43%. We assume that the obtained 10 % difference in porosity could change the mechanical properties for the implant materials prepared in the same conditions.

Changes in the HAp/Ag phase composition were identified by XRD using sintered powders and scaffolds. The results demonstrated that the phase composition depended on the sintering temperature (Table 2).

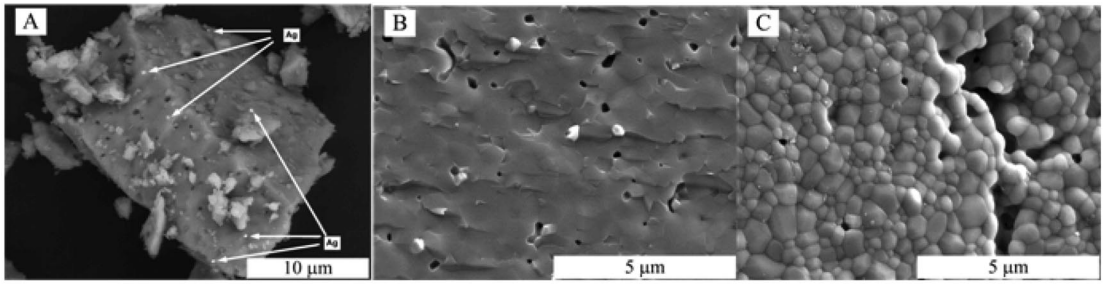

Fig. 2 SEM images of HAp/Ag2 sintered at 1150 °C: (A) particles, (B) scaffold fracture, and (C) scaffold surface.

Table 2 Phase composition changes in the sintering process.

	Detected phase composition by XRD					
	Scaffold surface (1000 °C)	Scaffold surface (1150 °C)	Milled scaffold (1000 °C)	Milled scaffold (1150 °C)	Powder (1000 °C)	Powder (1150 °C)
HAp/Ag1	HAp	HAp	HAp Ag AgO	HAp AgO	HAp AgO Ag	HAp AgO
HAp/Ag2	HAp	HAp	HAp Ag AgO	HAp Ag AgO	HAp Ag AgO	HAp Ag AgO

XRD analysis testified that the surface of the sintered scaffolds corresponded to pure HAp due to the silver evaporation during the sintering process. XRD patterns of sintered scaffolds at 1150 °C are compared in Fig. 3. Characteristic peaks of HAp are observed for all three samples.

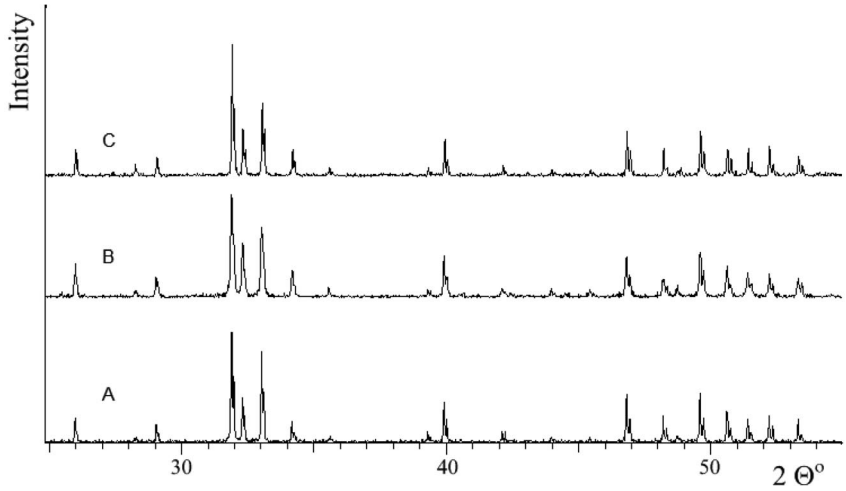

Fig. 3 XRD patterns of scaffolds surfaces sintered at 1150 °C: (A) Hap, (B) HAp/Ag1, and (C) HAp/Ag2.

SEM images of scaffold fractures indicated that the silver phase was distributed within the scaffold (Fig. 2). To determine the phase composition through the scaffold, scaffolds were milled in a mortar and used for further XRD analysis. Figure 4 shows a comparison of milled scaffolds and powder samples that were sintered at 1000 °C. These samples contained silver and silver oxide AgO phases; the characteristic peak of silver oxide was observed at 2θ 37.5° and the peaks of silver were observed at 2θ 38.2° and 44.4° for HAp/Ag2. The characteristic peak of silver at 2θ 44.4° was not observed for HAp/Ag1 samples due to the small amount of silver. The phase composition of HAp/Ag1 and HAp/Ag2 did not depend on the sample processing method, i.e., the phase composition of the scaffolds sintered at the same temperature was equal.

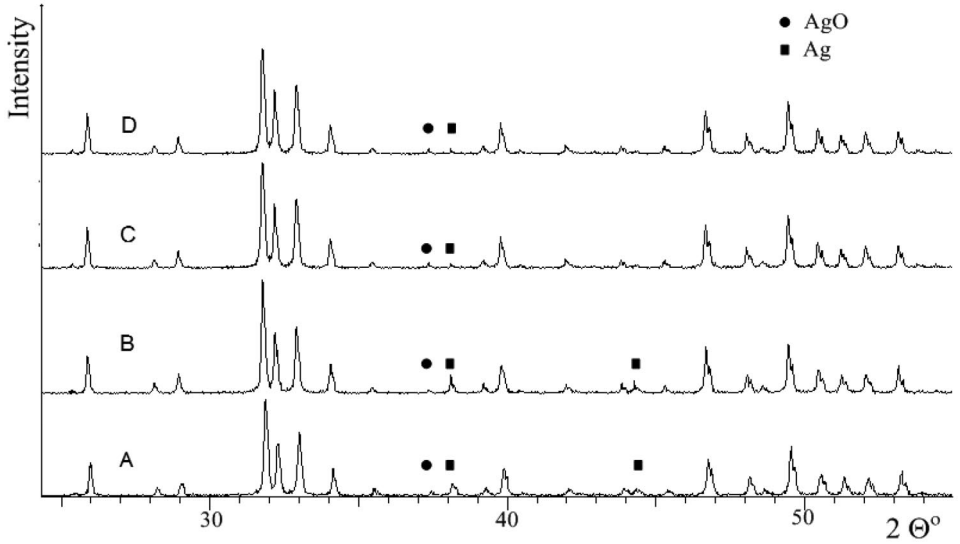

Fig. 4 XRD patterns of samples sintered at 1000 °C: (A) HAp/Ag2 milled scaffold, (B) HAp/Ag2 powder, (C) HAp/Ag1 milled scaffold, and (D) Hap/Ag1 powder.

With increasing sintering temperature up to 1150 °C, silver oxidized to AgO according to the reaction: $2Ag + O_2 \leftrightarrows 2AgO$ [28]. XRD patterns of sintered powders at both temperatures are compared in Fig. 5. The intensities of silver peaks at 2θ 38.2° and silver oxide peaks at 2θ 37.5° for HAp/Ag2 samples were higher in comparison with those for HAp/Ag1 samples due to the silver content in the samples. The intensity of the silver oxide peak at 2θ 37.5° grew, but that of the silver peak at 2θ 38.2° decreased with increasing sintering temperature up to 1150 °C, confirming the silver transformation to silver oxide.

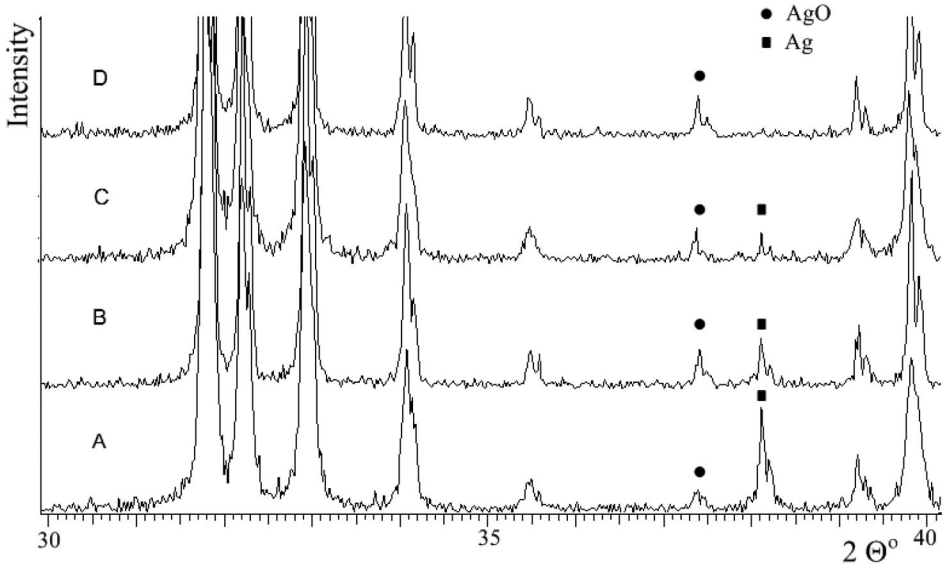

Fig. 5 XRD patterns of powder samples: (A) HAp/Ag2 sintered at 1000 °C, (B) HAp/Ag2 sintered at 1150 °C, (C) HAp/Ag1 sintered at 1000 °C, and (D) HAp/Ag1 sintered at 1150 °C.

Antibacterial activity of sintered scaffolds

The antibacterial activity of HAp, HAp/Ag1 and HAp/Ag2 scaffolds sintered at 1000 and 1150 °C toward *S. epidermidis* and *P. aeruginosa* bacterial strains was evaluated. The results showed that on the scaffolds sintered at 1000 °C, the adhesion of *S. epidermidis* began when the bacteria were incubated for 2 h at the concentration of 10^2 CFU/mL, while that of *P. aeruginosa* began at the concentration of 10^3 CFU/mL (Table 3).

Table 3 Intensity of adhesion.

	S. epidermidis CFU/mm^2			*P. aeruginosa* CFU/mm^2		
	10^1	10^2	10^3	10^1	10^2	10^3
HAp 1000 °C	0	0.0190 ± 0.0050	0.0910 ± 0.0026	0	0.0120 ± 0.0050	0.3760 ± 0.0350
HAp/Ag1 1000 °C	0	0.0120 ± 0.0050	0.0480 ± 0.0016	0	0	0.2730 ± 0.0300
HAp/Ag2 1000 °C	0	0.0060 ± 0.0002	0.0180 ± 0.0060	0	0	0.2420 ± 0.0300
HAp 1150 °C	0	0.0050 ± 0.0002	0.0350 ± 0.0018	0	0.0100 ± 0.0020	0.0700 ± 0.0050
HAp/Ag1 1150 °C	0	0	0.0150 ± 0.0050	0	0	0
HAp/Ag2 1150 °C	0	0	0.0050 ± 0.0002	0	0	0

SEM results showed that the samples containing pure HAp did not demonstrate any antibacterial activity. The colonization activity of *S. epidermidis* was inhibited on the silver-containing samples, especially on the samples sintered at 1150 °C (Fig. 6). It was observed that *S. epidermidis* formed dense colonies on biomaterials without silver, and some cells were connected to each other with glycocalyx. On the surface of biomaterials containing silver and sintered at 1000 °C, *S. epidermidis* formed colonies without glycocalyx, while only rare and separate bacterial cells with the absence of glycocalyx were found on the surface of silver, containing biomaterials sintered at 1150 °C (Fig. 7). This may suggest that biomaterials with silver (especially, sintered at 1150 °C) can be a better choice than biomaterials without silver for practical use to prevent device-associated infections.

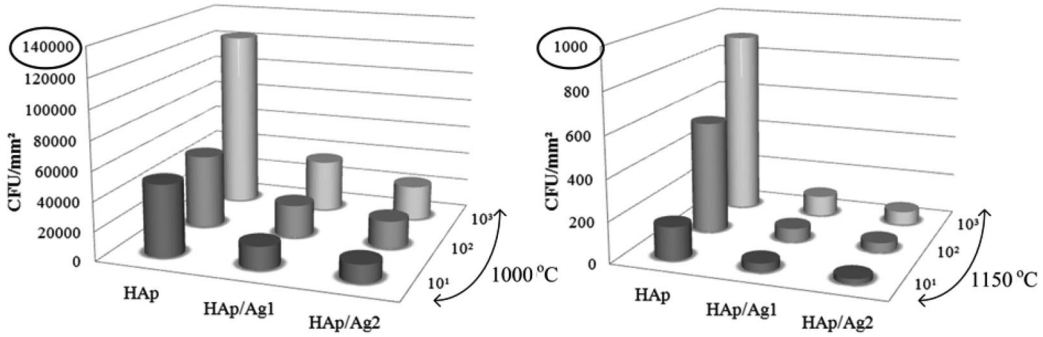

Fig. 6 Colonization intensity of *S. epidermidis.*

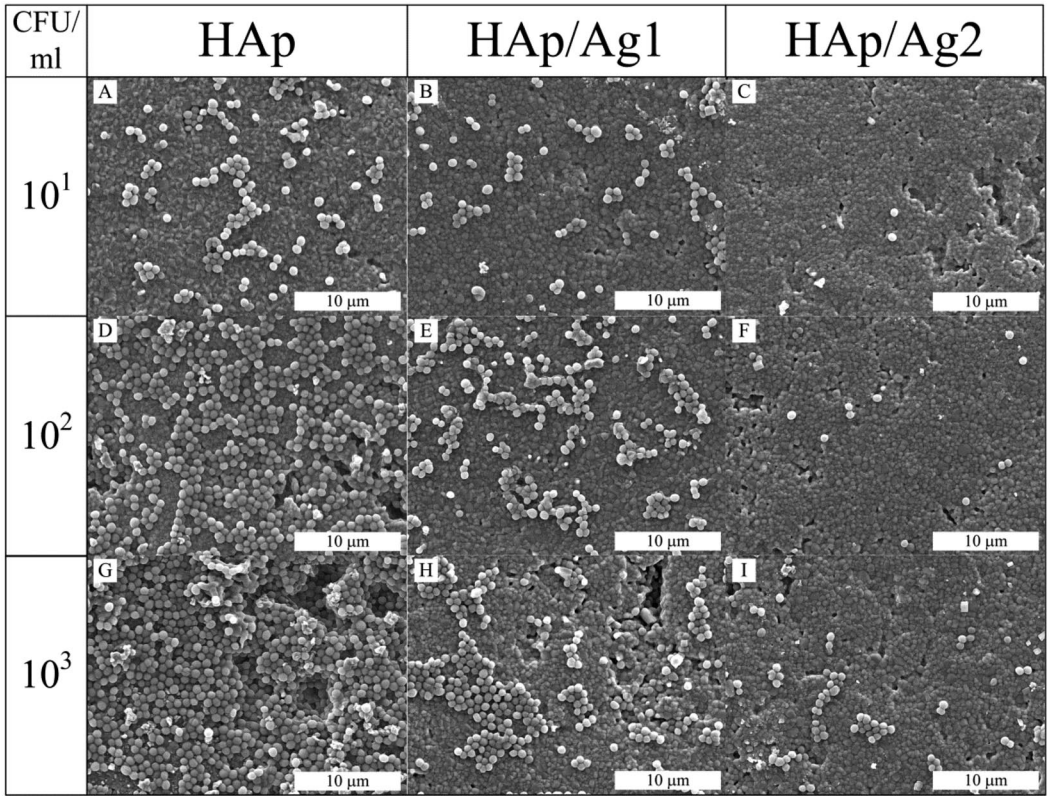

Fig. 7 Colonization intensity of *S. epidermidis* for scaffolds sintered at 1000 °C: (A, D, G) HAp, (B, E, H) HAp/Ag1, and (C, F, I) HAp/Ag2.

P. aeruginosa demonstrated a homogeneous growth on HAp biomaterials sintered at 1000 °C, and bacteria did not form colonies covered with glycocalyx. It was determined that the colonization intensity of *P. aeruginosa* (at a concentration of 10^3 CFU/mL) for samples sintered at 1150 °C significantly differed, namely, it was 23 ± 1 CFU/mm^2 for HAp/Ag2 but 49 090 ± 145 CFU/mm^2 for HAp (Fig. 8).

Colonization test results showed that the bacterial growth was limited on the samples containing silver and which were sintered at a temperature of 1150 °C. The pronounced inhibition of *Staphylococcus* and *Pseudomonas* colonization was observed on HAp/Ag2 samples.

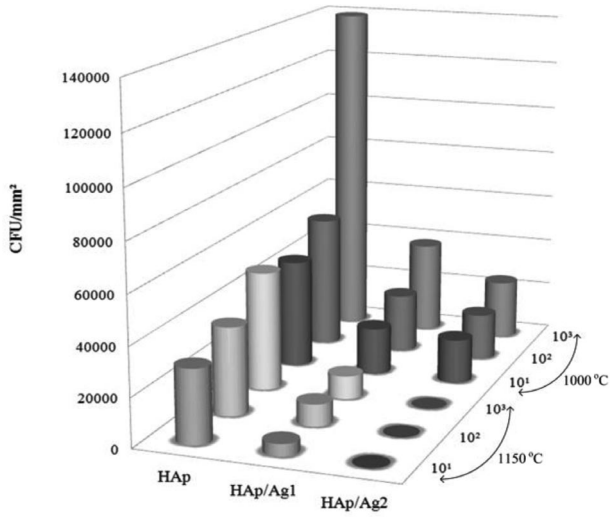

Fig. 8 Colonization intensity of *P. aeruginosa.*

CONCLUSIONS

The phase composition and phase transition of the HAp/Ag mixed crystal depends on the silver amount incorporated in the samples and the sample sintering temperature. With increasing Ag amount in the samples and sintering temperature, the porosity of the material decreases. HAp/Ag samples sintered at 1000 °C contain three phases, i.e., HAp, silver, and silver oxide ones. With increasing sintering temperature, silver oxidizes to silver oxide; therefore, HAp/Ag samples sintered at 1150 °C contain two phases. Samples containing pure HAp did not demonstrate any antibacterial activity, while samples containing silver and sintered at 1150 °C, in comparison with the HAp/Ag samples sintered at a temperature of 1000 °C, presented excellent antimicrobial properties.

ACKNOWLEDGMENT

This work has been supported by the European Social Fund within the project "Multidisciplinary Research in Biomaterials Technology of New Scientist Group", No. 2009/0199/1DP/1.1.1.2.0/09/APIA/VIAA/090.

REFERENCES

1. S. V. Dorozhkin. *Biomaterials* **31**, 1465 (2010).
2. D. Tadic, M. Epple. *Biomaterials* **25**, 987 (2004).
3. M. Vallet-Regi, J. M. Gonzalez-Calbet. *Prog. Solid State Chem*. **32**, 1 (2004).
4. H. Kawahara. *Clin. Mater.* **2**, 181 (1987).
5. E. Boanini, M. Gazzano, A. Bigi. *Acta Biomater.* **6**, 1882 (2010).
6. A. Ewald, D. Hosel, S. Patel, L. M. Grover, J. E. Barralet, U. Gbureck. *Acta Biomater.* **7**, 4064 (2011).
7. M. Bosetti, A. Masse, E. Tobin, M. Cannas. *Biomaterials* **23**, 887 (2002).
8. C. S. Ciobanu, F. Massuyeau, L. V. Constantin, D. Predoi. *Nanoscale Res. Lett.* **6**, 613 (2011).
9. X. Pang, I. Zhitomirsky. *Surf. Coat. Technol.* **202**, 3815 (2008).
10. V. Simon, C. Albon, S. Simon. *J. Non-Cryst. Solids* **354**, 1751 (2008).
11. X. Bai, K. More, C. M. Rouleau, A. Rabiei. *Acta Biomater.* **6**, 2264 (2010).

12. T. N. Kim, Q. L. Feng, J. O. Kim, J. Wu, H. Wang, G. C. Chen, F. Z. Cui. *J. Mater. Sci.: Mater. Med.* **9**, 129 (1998).
13. R. J. Chung, M. F. Hsieh, K. C. Huang, L. H. Perng, F. I. Chou, T. S. Chin. *J. Sol-Gel Sci. Technol.* **33**, 229 (2005).
14. J. K. Liu, X. H. Yang, X. G. Tian. *Powder Technol.* **184**, 21 (2008).
15. M. Diaz, F. Barba, M. Miranda, F. Guitian, R. Torrecillas, J. S. Moya. *J. Nanomater.* Article ID 498505 (2009).
16. Y. Chen, X. Zheng, Y. Xie, H. Ji, C. Ding, H. Li, K. Dai. *Surf. Coat. Technol.* **205**, 1892 (2010).
17. V. Stanic, D. Janackovic, S. Dimitrijevic, S. B. Tanaskovic, M. Mitric, M. S. Pavlovic, A. Krstic, D. Jovanovic, S. Raicevic. *Appl. Surf. Sci.* **257**, 4510 (2011).
18. B. Singh, A. K. Dubey, S. Kumar, N. Saha, B. Basu, R. Gupta. *Mater. Sci. Eng., C* **31**, 1320 (2011).
19. N. Rameshbabu, T. S. Sampath Kumar, T. G. Prabhakar, V. S. Sastry, K. V. Murty, K. Prasad Rao. *J. Biomed. Mater. Res. A* **80**, 581 (2007).
20. A. Afshar, M. Ghorbani, N. Ehsani, M. R. Saeri, C. C. Sorrell. *Mater. Des.* **24**, 197 (2003).
21. S. Catros, F. Guillemot, E. Lebraud, C. Chanseau, S. Perez, R. Bareille, J. Amédée, J. C. Fricain. *IRBM* **31**, 226 (2010).
22. A. Rapacz-Kmitaa, C. Paluszkiewicza, A. Ślósarczyk. *J. Mol. Struct*. **744–747**, 653 (2005).
23. K. Kalishwaralal, S. BarathManiKanth, S. R. K. Pandian, V. Deepak, S. Gurunathan. *Colloids Surf., B* **79**, 340 (2010).
24. C. Vuong, M. Otto. *Microbes Infect.* **4**, 481 (2002).
25. C. M. Toutain, N. C. Caizza, M. E. Zegans, G. A. O'Toole. *Res. Microbiol.* **158**, 471 (2007).
26. A. Trampuz, K. E. Piper, M. J. Jacobson. *N. Engl. J. Med.* **357**, 654 (2007).
27. M. F. Sampedro, P. M. Huddleston, K. E. Piper. *Spine* **35**, 1218 (2010).
28. G. Schon. *Acta Chem. Scand*. **27**, 2623 (1973).

